Modelling and design of stress–induced martensite formation in metastable β Ti alloys

Suresh Neelakantan [a,b,1,*], E.I. Galindo-Nava[e,c], David San Martin[d], Jesus Chao[d], P.E.J. Rivera-Díaz-del-Castillo[e]

[a] *Materials Innovation Institute, Kluyverweg 1, 2629 HS, Delft, The Netherlands*
[b] *Faculty of Aerospace Engineering, Delft University of Technology, Kluyverweg 1, 2629 HS, Delft, The Netherlands*
[c] *Faculty of Mechanical, Maritime and Materials Engineering, Delft University of Technology, Mekelweg 2 2628 CD, Delft, The Netherlands*
[d] *MATERALIA group, Dept. Physical Metallurgy, Centro Nacional de Investigaciones Metalurgicas (CENIM-CSIC), Av. Gregorio del amo 8, 28040 Madrid, Spain*
[e] *Department of Materials Science and Metallurgy, University of Cambridge, 27 Charles Babbage Road, CB3 0FS Cambridge, United Kingdom.*

Abstract

The temperature dependence of the stress-induced martensite (SIM) formation in a Ti-10V-2Fe-3Al (Ti-1023) alloy under compressive loading has been studied. At low temperatures, the stress level at which martensite starts to form increases linearly with the deformation temperature, while the stress at which the deformation switches to regular plastic deformation is roughly temperature independent. A thermostatistical model for dislocation evolution is employed to describe deformation twinning in martensite. Combined effects of twinning induced plasticity and solid solution strengthening are considered in terms of temperature variations. The SIM effect disappears on deformation at temperatures beyond ∼233 °C, which is close to the predicted M_s temperature of 240 °C. The thermostatistical model predicts a transition from twinned martensite to pure slip at 250 °C. By providing a model to predict stress induced martensite formation, and by describing deformation twinning, the present work provides a number of tools that may be employed to conceive new titanium alloys combining improved strength and ductility.

Keywords: Titanium alloys, Twinning, Stress-induced martensite, High temperature

*Author's current position is in Department of Engineering, University of Cambridge, Trumpington Street, Cambridge CB2 1PZ, United Kingdom

Email address: pejr2@cam.ac.uk (P.E.J. Rivera-Díaz-del-Castillo)

[1] Most of the experimental work was performed during author's position at Faculty of Aerospace Engineering, Delft University of Technology, Kluyverweg 1, 2629 HS, Delft, The Netherlands.

deformation, Dislocations

1. Introduction

Several challenges are faced by titanium alloys towards their commercialisation and widespread use. Although recent progress has been made in their cost reduction, issues such as strong texture and poor formability remain a challenge [1]. A way to increase formability is by exploitation of their ability to form martensite under stress around room temperature. Athermal martensite forms on quenching from a high temperature phase, inducing a phase transformation triggered by the co–ordinated production of stacking faults. This process has been described by Olson and Cohen for a variety of parent (high temperature phase) and product (martensite) crystal structures [2, 3, 4]. The product phase formed on quenching undergoes only *incomplete* transformation, as this is arrested by the adjoining high temperature phase, which becomes retained when quenching to room temperature. Further martensite formation becomes possible at low temperature by supplying an extra amount of energy by mechanical means. This is referred to as *stress–induced martensite* (SIM), which deformation may lead to concomitant improvements in strength and ductility, as has been demonstrated in steel technology [5].

SIM formation is a widely observed phenomenon in β and near β titanium alloys [6, 7, 8, 9, 10]. A sufficiently high level of β stabilising elements hinders the diffusional β (austenite) to α phase transformation, leading to a metastable β, which potentially can transform to martensite or ω phase [11, 12, 13]. The transformation from metastable β to martensite can occur either athermally or under the influence of stress, depending on alloy composition and deformation temperature, which eventually determines the SIM formation capability. Recent studies have shown that the SIM effect can be tailored to achieve improvements in the mechanical properties of the near β-Ti-10V-2Fe-3Al (Ti-1023) alloy [14]. The key factor which controls the deformation induced martensite formation at room temperature is the composition of the β (austenite) phase, which determines its metastability and M_s temperature. The composition of the β phase itself is defined by the heat treatment conditions. The range of heat treatment conditions leading to enhanced metastability of the β phase, required to trigger martensite formation upon deformation at room temperature, have been

identified for the Ti-1023 alloy [14]. Such treatments resulted in an increase of the compressive strength by ∼20 % due to the presence of SIM [14]. However, little is known about the temperature dependence of the SIM phenomenon and its relation to the athermal M_s temperature. Additionally, by assuming that martensite plays a dominant role during work hardening, a thermodynamics–based deformation twinning model (for hexagonal metals) is employed to describe the experimental stress–strain curves. Central to this approach, is the introduction of the statistical entropy accounting for the possible dislocation migration paths. This allows to obtain an expression for the dislocation recovery term as a function of the energy barrier for dislocation annihilation [15]. Based on a Kocks–Mecking formulation, a dislocation density evolution equation has been derived to characterise solid solution effects. On the other hand, deformation twinning in pure hexagonal materials has been described by incorporating an additional dislocation generation term for twin propagation [16]. Such term becomes active once a critical strain for twin nucleation is reached. The current work aims at describing, both experimentally and theoretically, the temperature dependence of the SIM properties in metastable β Ti-1023 alloy and the transition temperature from SIM deformation mode to regular plastic deformation via dislocation motion. The model combines multicomponent and deformation twinning effects for describing twinning deformation in martensite. The capacity to apply this concepts for the conception of titanium alloys of improved strength and ductility is discussed.

2. Thermostatistical model for plasticity

2.1. Energy barrier for dynamic recovery

The Kocks–Mecking equation [17], has recently been subjected to a thermodynamic analysis [15] aimed at obtaining expressions for the dynamic recovery rate f_{DRV}, in terms of an annihilating dislocation segment (of length l).

$$\frac{d\rho(\gamma)}{d\gamma} = \frac{d\rho^{+}}{d\gamma} - f_{DRV}\rho(\gamma), \tag{1}$$

where ρ is the average dislocation density, γ is the shear strain, and $\frac{d\rho^{+}}{d\gamma}$ is the dislocation generation rate (presented in the following sections). Such analysis leads to an expression for f_{DRV} in terms of

an energy barrier for dislocation annihilation $\langle \Delta G \rangle$ in multicomponent systems. $\langle \Delta G \rangle$ is composed by the addition of five terms [15]:

1. A dislocation formation energy term, approximated by the strain energy around the annihilating segment: $U_{form} = \frac{1}{2}\mu b^2 l$, where μ is the shear modulus and b is the magnitude of the Burgers vector.
2. A migration energy term: $U_{mig} = \sigma_Y A_{act} b^2 l$, where σ_Y is the yield stress, and A_{act} is the (dimensionless) activation area for cross-slip.
3. A vacancy energy contribution to dislocation annihilation at higher temperatures (via dislocation climb), induced by the vacancy chemical work around the segment: $U_{vac} = \frac{V_{sys}}{b^3}\delta\big(E_f + k_B T \ln c_m\big)$, where $V_{sys} = l^* l b$ is the volume of the annihilating system (a dislocation distortion's field length on a slip plane), $l^* = 12.5b$ is the dislocation's distortion field length ($\sim$98% of the total strain field induced by the dislocation [18]); E_f is the vacancy formation energy, c_m is the vacancy concentration at the melting point (T_m), and $\delta(T)$ is a continuum piecewise function that vanishes the vacancy contribution ($\delta = 0$) at low temperatures[2]($T < T_0$), increases linearly at medium temperatures ($T_0 < T < T_f$), and becomes fully present ($\delta = 1$) at high temperatures ($T > T_f$).
4. A dislocation–solute atom interaction energy term, approximated by the solute chemical potential around the segment: $U_{SS} = V_{sys} \sum_i x_i \Delta G_{sys}$, where x_i is the atomic fraction of the i solute element, and ΔG_{sys} is the free energy of the mixture.
5. A statistical entropy contribution $T\Delta S$ accounting for the energy dissipation due to the energetically *favourable* dislocation paths active during deformation.

The additions of these terms leads to

$$\langle \Delta G \rangle = \frac{b}{l}\big(U_{form} + U_{mig} + U_{vac} + U_{SS} - T\Delta S\big), \tag{2}$$

where the factor b/l scales the energy contributions to the number of particles along the dislocation line participating in the annihilation process. In a thermally activated process, the expected velocity

[2]Definitions of T_0 and T_f are presented in section 2.3.

for a dislocation to undergo annihilation can be expressed in terms of an Arrhenius equation, where $\langle \Delta G \rangle$ is the energy to be overcome. Combining the previous expressions, l can be obtained. A detailed analysis on how to derive l can be found in [18].

2.2. Quantification of the number of microstates

Instead of trying to describe the instantaneous velocity gradient at every moment, the entropy accounts for the total energy loss due to the different dislocation velocity configurations. A microstate is defined as the number of interatomic subunits a dislocation segment can glide during an arbitrary time step Δt [18]. At high temperatures, vacancy-dislocation interactions become prominent, increasing dislocation motion events via vacancy-assisted climb and consequently additional number of microstates are incorporated [19]. The total number of microstates (dislocation slip+climb) Ω becomes [18, 19]:

$$\Omega = \Omega_{dis} + \Omega_{v-d} = \left(\frac{\dot{\varepsilon}_0 + \vartheta}{\dot{\varepsilon}} \right), \tag{3}$$

where Ω_{dis} and Ω_{v-d} are the number of microstates due to dislocation slip and to vacancy-dislocation interaction respectively; $\dot{\varepsilon}_0 = cb\rho_Y$ is a limiting value for strain rate, this is achieved when the dislocations approach the speed of sound in the material, c; ρ_Y is the dislocation density consistent with the yield point ($\rho_Y = (\sigma_Y / 0.9\mu b)^2$ [18]); $\dot{\varepsilon}$ is the strain rate; $\vartheta = \vartheta_D \exp\left(-\frac{E_m}{RT}\right)$ is the vacancy migration frequency, wherein $\vartheta_D = 10^{13}$ s^{-1} is the Debye frequency, E_m is the vacancy migration energy, R is the gas constant and T is the absolute temperature.

2.3. Low and high temperature deformation regimes

The transition temperatures for different dislocation annihilation mechanisms are obtained by comparing Ω_{dis} and Ω_{v-d} [19]: $T_0 = \frac{E_m}{R \ln(\vartheta_D / \dot{\varepsilon})}$, when only one vacancy–dislocation interaction microstate is available; and $T_f = \frac{E_m}{R \ln(\vartheta_D / \dot{\varepsilon}_0)}$, when vacancy–dislocation microstates equal those for pure slip. Below T_0 no vacancy effect is present and cross-slip is the main annihilation mechanism; above T_f vacancy-assisted dislocation climb is the predominant annihilation mechanism; and between these values, both mechanisms take place. In pure FCC and HCP metals it has been found that $0.2T_m \leq T_0 \leq 0.3T_m$ and $0.5T_m \leq T_f \leq 0.6T_m$, being these values in good agreement with the transition ranges usually considered in the literature [16, 19].

Table 1: Chemical composition (in wt.%) of the Ti-1023 alloy.

Alloy	Al	V	Fe	O	N	C	Ti
Ti-1023	3	9.8	1.9	0.11	0.01	0.007	bal.

2.4. Entropy and dynamic recovery rate

The statistical entropy for pure metals equals [18]:

$$\Delta S = k_B \ln \Omega = k_B \ln \left(\frac{\dot{\varepsilon}_0 + \vartheta}{\dot{\varepsilon}} \right). \tag{4}$$

The dynamic recovery term equals the fraction of substance undergoing dislocation annihilation per dislocation and is given by [15]:

$$\begin{aligned} f_{DRV} &= \frac{N_A}{w_a}\rho_a V_{sys} = \frac{N_A}{w_a}\rho_a b l^* l \\ &= \frac{N_A \rho_a b^2 l^* (w_a^{-1})(1+\Phi_{SS}b^3)\mathcal{N}T\Delta S}{\frac{1}{2}\mu b^3 + \sigma_Y A_{act} b^3 + \frac{l^*}{b}\delta\big(E_f + k_B T \ln c_m\big) + l^* b^2 \sum_i x_i \Delta G_{sys} - k_B T \ln\left(\frac{\dot{\varepsilon}_0+\vartheta}{\dot{\varepsilon}}\right)^{\mathcal{N}}}, \end{aligned} \tag{5}$$

where N_A is the Avogadro's number; ρ_a is the alloy's density; w_a is the atomic weight; $\Phi_{SS} = \sum x_i/b^3$ is the solute concentration per unit volume; and $\mathcal{N}$ is an additional annihilation effect due to the overlapping strain field of contiguous dislocations that alters the expected velocity for dislocation motion [18][3]. The term $(1+\Phi_{SS}b^3)$ in the numerator accounts for the additional number of microstates (barriers) generated by the interaction of dislocations with solute atoms.

The theory is able to describe deformation by slip in concentrated solutions only. However, twinning occurs in martensite phase of Ti alloys [20]. Combined effects of diluted solid solution (*e.g.* V, Al, Fe) and deformation twinning are derived in this work.

3. Experimental procedure

Forged and heat treated β-Ti-10V-2Fe-3Al (wt.%) material was provided by TIMET, Germany. The composition of the alloy, as reported by the supplier, is shown in Table 1. The β-transus temperature of the alloy was determined to be 795 ± 5 °C using dilatometry [6, 14]. The as-received material,

[3] $\mathcal{N}$ is related to the stacking fault energy. A detailed analysis on how to estimate $\mathcal{N}$ can be found in [18].

machined to 7 mm (h) × 4 mm (d) cylindrical samples, was subjected to a 900 °C – 3600 s solution treatment before mechanical testing, yielding a microstructure with metastable β and athermal martensite (mainly restricted to the neighbourhood of grain boundaries). Complete details of the microstructure and its corresponding phases for the considered solution treatment condition can be seen in Figures 1 and 2 of reference [14]. The heat treatments were performed on a Bähr 805 horizontal dilatometer at a vacuum level of 10^{-5} mbar, and the material was quenched to room temperature by Helium gas flow [14]. The homogenised samples were subsequently compressed to a total strain of at least 30% in the same deformation dilatometer (load cell capacity of 20 kN) at a fixed strain rate of 1.4×10^{-3} s^{-1} at various temperatures ranging from 33 °C to 400 °C (33, 93, 163, 183, 213, 233, 293, 350, 375 and 400 °C). The deformation temperature was maintained within an accuracy of ± 5 °C. All samples have been characterised after compression using X-ray diffraction (XRD) with Co K_α radiation at room temperature.

4. Model for multicomponent deformation twinning

4.1. Multicomponent effects

A high dislocation dissociation rate is present in the martensite phase (HCP) in Ti-10V-2Fe-3Al due to the reduced number of slip systems [16]. As deformation continues, the glide of partial dislocations in the HCP phase leads to twin boundary formation, increasing the work hardening rate via additional dislocation generation. This term contains a delay due to the strain required for twin nucleation. It is proposed that $\frac{d\rho^+}{d\gamma}$ in equation 1 incorporates the dislocation generation contributions of:

1. Dislocation–dislocation interactions in the pure material $\Lambda_{pure}^{-1} = k_1\sqrt{\rho(\gamma)}$, where Λ_{pure} is the dislocation mean free path in a pure metal, $k_1 = \frac{1}{30}\left(\frac{\mu}{\mu_0}\right)^2$ and μ_0 is the shear modulus at 0 K.
2. Dislocation–solute atom interactions $\Lambda_{SS}^{-1} = k_{SS}\sqrt{\rho(\gamma)}$, where Λ_{SS} is the dislocation mean free path in the presence of solute strengtheners, and k_{SS} is a constant.
3. Twin nucleation and growth $\Lambda_T^{-1} = k_T\sqrt{\rho(\gamma - \gamma_T^*)}$, where Λ_T is the average twin thickness, k_T is a constant and γ_T^* is the critical strain for twin nucleation.

The dislocation evolution equation then becomes:

$$\frac{d\rho(\gamma)}{d\gamma} = \frac{1}{b}\left(\frac{1}{\Lambda_{pure}} + \frac{1}{\Lambda_{SS}} + \frac{1}{\Lambda_T}\right) - f_{DRV}\rho(\gamma) = \frac{k_1 + k_{SS}}{b}\sqrt{\rho(\gamma)} + \frac{k_T}{b}\sqrt{\rho(\gamma - \gamma_T^*)} - f_{DRV}\rho(\gamma), \quad (6)$$

k_{SS} has been obtained for concentrated solutions [15]:

$$k_{SS} = \frac{\Phi_{SS} b^3}{16000} \exp\left(-\frac{\Delta G_{sys}}{RT}\right), \quad (7)$$

whereas k_T has been described for deformation twinning in pure hexagonal metals only. This work presents a combination of solid solution and deformation twinning effects in the martensite phase.

4.2. Twin nucleation strain

In previous work, it has been proposed that twin nucleation occurs when the addition of the dislocation forest energy (E_{forest}) and the (displacement) energy of moving dislocations towards piling up (E_{disp}), equals the addition of the strain energy to form a twin embryo (E_{nucl}) and the excess strain energy around the embryo to ignite propagation (E_{exs}) [16]:

$$E_{forest} + E_{disp} = E_{nucl} + E_{exs}. \quad (8)$$

The energy of a dislocation forest equals [21]: $E_{forest} = \frac{n_f}{2}\mu b^2 \bar{l}$, where n_f is the number of dislocations in the forest and $\bar{l}$ is the average dislocation spacing. The displacement energy equals the statistical entropy accounting for the dislocation migration paths [16]: $E_{disp} = n_f \frac{\bar{l}}{b} T\Delta S$. E_{nucl} represents the strain energy around a newly formed twin embryo, requiring n^*_{nuc} dislocations to split into Shockley partials: $E_{nucl} = \frac{n^*_{nuc}}{2}\mu b^2 \bar{l}$. n^*_{nuc} is approximated by the ratio between the area surrounded by a twin embryo with an initial boundary length $\overline{x}_T$ (and thickness b), and the equivalent area of the forest in the absence of twins ($\bar{l}^2$)[16]:

$$n^*_{nuc} = \frac{2\overline{x}_T b}{\bar{l}^2} n_f, \quad (9)$$

where the factor of 2 accounts for the duplicity in twin boundaries. E_{exs} is proportional to the energy fraction of dislocations piling-up around the embryo (S_T): $E_{exs} = \beta_1 S_T E_{forest}$, where β_1 is a constant depending on the twin and slip configurations and material. If a twin embryo is assumed

to have a circular cross-section, with diameter equal to the distance between partials (r_{part}), S_T is proportional to the perimeter of the embryo per unit area $S_T = \frac{P_T b}{A_T} = \frac{\pi r_{part} b}{\pi r_{part}^2/4} = \frac{4b}{r_{part}}$, where P_T and A_T are the perimeter and area of the embryo, respectively. Combining and rearranging the previous expressions, and employing $r_{part} = \frac{(2+\nu)\mu b^2}{24\pi(1-\nu)\chi}$ [22], where χ is the stacking fault energy and ν is the Poisson ratio, the critical strain γ_T^* for twin nucleation equals

$$\gamma_T^* = \overline{x}_T b\rho = \left(\frac{1}{2} + \frac{T\Delta S}{\mu b^3} - \beta_1 \frac{96\pi(1-\nu)\chi}{(2+\nu)\mu b}\right), \tag{10}$$

with $1/\bar{l} = \sqrt{\rho}$ and $\gamma_T^* = \overline{x}_T b\rho$ is an Orowan–type equation [15]. Once γ_T^* is reached, the twinning deformation term in equation 6 becomes active. If $\gamma_T^* \leq 0$ then $\gamma_T^* = 0$. A physical interpretation of this condition is that the stored energy at yielding is high enough to nucleate twins.

4.3. Twinning coefficient

Twin growth requires additional dislocation storage at the boundaries E_{stored} to drive their propagation. E_{stored} requires to overcome the strain energy E_{twin} of the additional twin length plus the dissipated energy by moving boundaries E_{prop} [16]

$$E_{stored} = E_{twin} + E_{prop}. \tag{11}$$

E_{stored} is proportional to the strain energy of n_{TB} dislocations piling-up at the twin boundaries: $E_{stored} = \beta_2 \frac{n_{TB}}{2} \mu b^2 \bar{l}$, where β_2 is a constant. E_{twin} corresponds to the strain energy of the additional twin platelet [16]: $E_{twin} = \beta_3 \bar{l}_T S_V \frac{n_{TB}}{2} \mu b^2 \bar{l}$, where S_V is the twin area per unit volume to account for the increase in the twin surface [15]: $S_V = A_T/V_T = 6/\Lambda_T$ (A_T and V_T are the twin area and volume, respectively); $\bar{l}_T = 1/\sqrt{\rho(\gamma - \gamma_T^*)}$ is the average dislocation spacing in the twins (interiors+boundaries)[4]; and β_3 is a material constant. The boundary propagation energy equals E_{disp} of n_{TB} dislocations [16]. Rearraning the previous expressions, k_T equals [16]:

$$k_T = \frac{\bar{l}_T}{\Lambda_T} = \frac{1}{6\beta_3}\left(\beta_2 - \frac{2T\Delta S}{\mu b^3}\right). \tag{12}$$

[4]Note that $\bar{l}_T$ contains a delay as it features only after twin nucleation occurs.

If $k_T \leq 0$ then it is fixed to 0 and no deformation twinning is favourable [16]. The factor $(6\beta_3)^{-1}$ accounts for the shape of the twin platelet.

4.4. Multicomponent dilute solutions

At moderate concentrations, a dislocation in a randomly dispersed solute atom field is subjected to interaction forces from the nearest effective solute atoms, undergoing repulsive or attractive motion. However, at low concentrations, a dislocation encounters only discrete and spread opposing obstacles (solute atoms), and their interaction is similar to the non–deformable particles case (*e.g.* precipitates acting as point–like obstacles)[22, 23]. The strengthening effect is related to the ability of dislocations to bow around the particles, and it depends on the average particle spacing only, rather than their spatial distributions [23]. Thus, it is proposed that instead of describing the volumetric interactions between solute atoms and dislocations in ΔS and Λ_{SS}, linear interactions are responsible for the strengthening and annihilation process: $\Phi_{SS}b^3$ is replaced by the solute concentration per unit length $\psi_{SS} = \sum x_i^{1/3}/b$ multiplied by b in equations 5 and 7. No modifications are made in the twinning formulation as the solid solution effect is implicitly incorporated in β_1, β_2 and β_3.

5. Results

5.1. Temperature–dependent plasticity

Compressive stress-strain curves obtained at the various deformation temperatures are shown in Figure 1. The double-yield behaviour, a phenomenon associated to SIM formation, disappears as the deformation temperature is increased. The low temperature stress-strain curves (33, 93, 163, 183 and 213 °C) distinctly show the double-yield points, which correspond to the martensite formation stress (or so called triggering stress [6]) and the slip stress (corresponding to regular plastic deformation due to dislocation motion), respectively. For deformation temperatures at or above 233 °C only a single yield point corresponding to regular slip deformation is observed.

The temperature dependence of the two critical stress levels, the martensite formation stress (σ_m, i.e. the first yield point) and the slip deformation stress (σ_s, i.e. the second yield point) is shown in Figure 2. The two critical stress values have been determined by the method of tangents

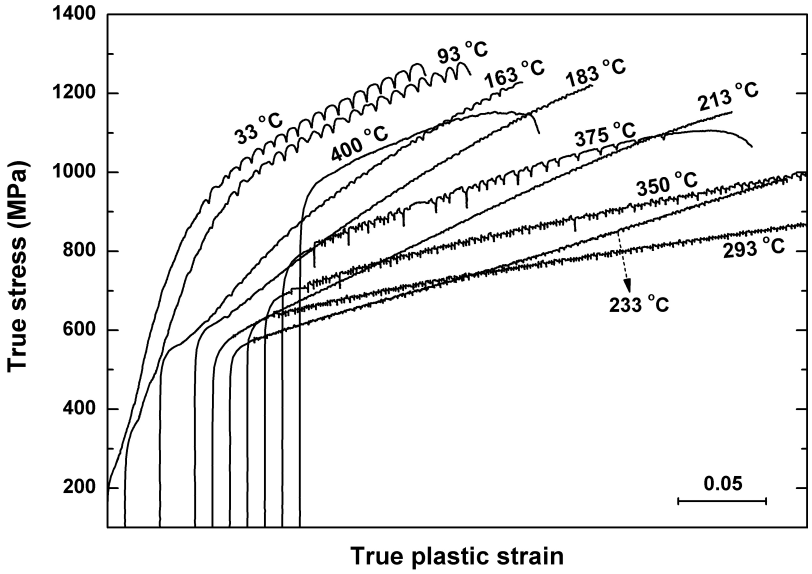

Figure 1: Compressive stress-strain curves of Ti-1023 alloy at various deformation temperatures. Onset of the curves have been shifted to discriminate the various curves more clearly.

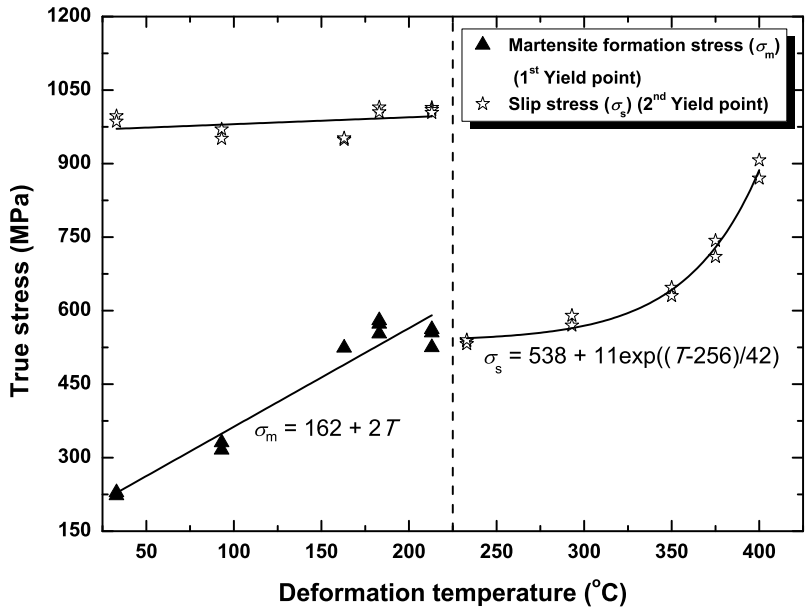

Figure 2: The critical stress values of the double-yield phenomenon as function of deformation temperature. The dotted line signifies the different deformation behaviour below and above the transition temperature of 233 °C.

intersection from the derivative of the stress-strain curves. The figure shows that the deformation behaviour is intrinsically different below and above the transition temperature of 233 °C. The dotted line in Figure 2 signifies this.

Below 233 °C, where the double-yield effect is evident, the slip deformation stress is roughly temperature independent, while the martensite formation stress increases more or less linearly with temperature. As a result, the separation between two yield points decreases with increasing deformation temperature, Fig. 2. Such observation quantitatively reflects the amount of SIM formation. The increase in deformation temperature increases the stability of the β phase fraction. Hence more energy is required to induce martensitic transformation leading to an increase of the martensite formation stress. The dependence of σ_m on the deformation temperature (T) can be approximated by a simple linear relation $\sigma_m = 162 + 2T$, where T is in °C, and σ_m is expressed in MPa. The slope ($d\sigma_m/dT = 2$ MPa/°C) can be related to the Clasius-Clapeyron equation also valid for shape memory alloys [24]. However, previous work by Duerig *et al.* [6] has shown that the linear dependence of the martensite formation stress (σ_m) does not apply below room temperature. Moreover, Patel and Cohen [25] have analysed the role of the applied stress (σ) during martensitic transformations. Such is based on performing a thermodynamic balance between the chemical driving force for the phase transformation occurrence (ΔF) and the mechanical work (W_{appl}) induced around a martensite platelet; from this balance the slope between σ and the transformation temperature ($d\sigma/dT$) is obtained. W_{appl} equals [25][5]: $W_{appl} = -\frac{\sigma}{2}(\gamma_0 \sin(2\theta) \pm \epsilon_0(1 + \cos(2\theta)))$ J m^{-3} where γ_0 and ϵ_0 are the shear and axial strains around the martensite platelet during the displacive transformation, respectively, and $\theta = \gamma_0/\epsilon_0$ is the angle between the specimen axis and the normal to any potential habit plane; the positive and negative signs in the second term of W_{appl} are for uniaxial tension and compression conditions, respectively. $d\sigma/dT$ equals:

$$\frac{d\sigma}{dT} = \frac{\frac{d\Delta F}{dT}}{\frac{dW_{appl}}{d\sigma}}. \tag{13}$$

For the present alloy, γ_0 and ϵ_0 can be estimated with the austenite and martensite lattice pa-

[5]The negative sign is included as the compressive stress is considered positive in this work.

rameters obtained in previous work [14]: $a_\beta = 0.323$ nm and $a_{mart} = 0.297$, $b_{mart} = 0.498$ and $c_{mart} = 0.439$ nm. ΔF was obtained from Thermocalc for various temperatures (within the range of the experiments); a linear expression was fitted to obtain the temperature slope: $\frac{d\Delta F}{dT} = 7.4$ J mol^{-1}°C^{-1}. In order to match the units of $\frac{d\Delta F}{dT}$, $\frac{dW_{appl}}{d\sigma}$ is multiplied by the molar volume of the alloy $V_{mol} = 1.02\times10^{-5}$ m^3 mol^{-1}. Thus, the stress slope with temperature predicted by equation 13 equals 1.76 MPa/°C; this value is close to the one obtained for σ_m from the experimental fitting. This criterion aids in providing a fundamental description in σ_m variation with temperature; it also confirms that additional mechanical work is required at higher temperatures for stress–induced martensite formation. Further analysis can be made in future work to combine the previous analysis with a yielding criterion for this alloy family. Equation 13 also shows that the martensite formation stress can be different for tension and compression loading.

Around 233 °C, where only single yield behaviour is observed, the slip initiation stress falls sharply to levels comparable to the martensite formation stress observed at or below 213 °C. With further increase in deformation temperatures a steady increase in the slip deformation stress values is observed. Such increase can be approximated by $\sigma_s = 538 + 11\exp((T-256)/42)$ relation, where T is in °C, and σ_s is expressed in MPa. The increase in slip initiation stress is ascribed to the β phase remaining stable, losing metastability, during deformation. Furthermore, at higher deformation temperatures some α phase may form leading to a further increase in the stability of the β phase. The occurrence of SIM formation during deformation has also been quantified using X-ray diffraction. To determine the relative amount of β (austenite) and martensite phase from the area of the relevant diffraction peaks (inset figure of Fig. 5.2), MDI Jade 5.0 software (Materials Data Inc, Livermore, CA, USA) has been used. An analysis on the diffractograms of samples compressed at various temperatures confirmed that the peak area of the stress-induced martensite peaks decreased with temperature to disappear after ∼233 °C (Fig. 5.2). Attention was focused on all diffraction peaks in the 2θ range from 40 until 110 degrees. It is worth to note that the low angle diffraction peaks (*i.e.* 2θ between 40 to 50 degrees) exhibited clear transformation trends. Moreover, the diffractograms show a concurrent increase in the amount of residual β (austenite) phase fraction after deformation at high temperatures. Further, at higher deformation temperatures

i.e. above 250 °C, the equilibrium α phase formation is observed.

It is interesting to note that the stress–strain curves in Fig. 1 display serrations after the second yield point, or once plastic deformation starts for temperatures above 213 °C. Since the serrations form once martensite has fully formed, they cannot be attributed to the transformation process. The amplitude of the serrations decreases with temperature, a behaviour consistent with the Portevin–Le Chatelier effect, with faster diffusion of solute towards dislocations as deformation takes place.

5.2. M_s prediction

It is interesting to assess whether the temperature at which the double yield disappears can be related to the athermal M_s temperature of the alloy. According to a recent thermodynamic model for binary Ti-X alloys [26], the M_s temperature of Ti-X (where X = Fe, Mn, Cr, Mo, Ni, Cu, V, Nb, Zr and Al) depends on the alloy concentration. By applying this model to multicomponent β titanium alloys, a good correlation between the predicted M_s temperature and the Mo equivalence, which is a measure of the β (meta-) stability for β Ti alloys [27, 28], is observed. Using this equation, the M_s temperature for the nominal composition of Ti-1023 alloy is predicted to be ∼240 °C [26]. This temperature coincides remarkably well with the temperature (∼233 °C) where the double yield effect due to SIM formation disappears (Figures 1 and 2).

5.3. Modelling deformation twinning in martensite

The model is tested against the experimental results for different temperatures and at a strain rate of 10^{-3} s^{-1}. It is assumed that the martensite phase mainly controls the alloy's work hardening behaviour after reaching the first yield point. In order to obtain the physical input parameters of this alloy, a mixture rule is used for b, μ, c, w_a and ρ_a, as no information was found in the literature [15]: $P = (1 - \sum_i x_i)P_{(1-\sum_i x_i)} + \sum_i x_i P_{x_i}$, where P_{x_i} and x_i represent the physical parameter and composition values of the i-th element[6], respectively. For the case of the vacancy migration and formation energies, they were taken equal to the value for pure Ti; this also implies that $T_0 = 409$ K and $T_f = 1096$ K correspond to the same values for pure Ti [16]. The stacking fault

[6]Weighted contributions are computed expressing x_i in atom fraction.

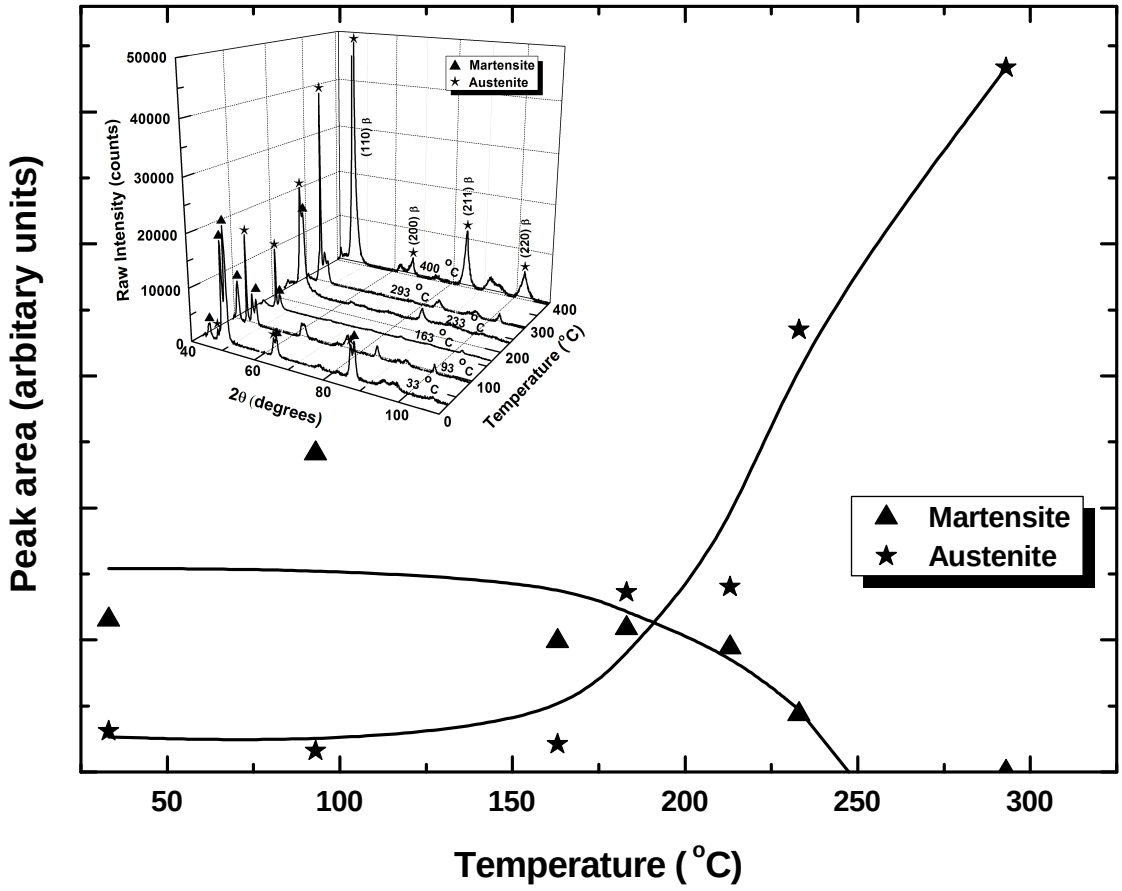

Figure 3: A quantitative measure of martensite and β (austenite) peak areas in deformed samples as function of deformation temperature. Above ∼233 °C temperature (from Figure 2) no martensite was found. The Inset shows the diffractograms of deformed samples, from which the martensite and austenite peak areas were obtained, for selected deformation temperatures.

Table 2: Material parameters.

Metal	b (nm)	c (m/s)	w_a (g/mol)	ρ_a (g/m^3)	μ (GPa)	E_m (eV)	E_f (eV)
Ti	0.29	5090	47.8	45	$53 - 0.03T$	1.3	2.1
V	0.263	4560	50.9	60	$56 - 0.015T$		
Fe	0.258	5120	55.8	78.9	$122 - 0.02T$		
Al	0.286	5000	26.9	27	$29.4 - 0.015T$		

energy was fitted to 100 mJ m^{-2}. Table 2 shows the values of the physical parameters employed in the model. b, c, w_a and ρ_a were obtained from [29]; μ was previously obtained and fitted to a formula to capture temperature variations; for Ti it was obtained from [16], for V and Fe from [30] and for Al from [19]; E_m and E_f were obtained from [31]. The values of ΔG_{sys} were obtained from Thermocalc and fitted to a formula to simplify the calculations: $\Delta G_{sys} = -(8880 + 12T + 0.03T^2)$ J/mol. Substitutional solid solution effects on Ti are considered for V, Al, and Fe. The effect of interstitial atoms (C and N) was not included in the model.

The fitting parameters are $\beta_1 = 2.25$, $\beta_2 = 0.958$ and $\beta_3 = 0.4174$. It is worth noting that in the case of pure materials, β_2 and β_3 can be expressed in terms of the angle between the predominant slip and twin planes, and no fitting is required [16]. The dislocation density is obtained by solving equation 6, with an initial density $\rho_0 = 10^{11}$ m^{-2}. The flow stress evolution is described by the Taylor equation [15]: $\sigma = \sigma_Y + \alpha\mu b\sqrt{\rho}$, where $\alpha = 0.3$ is a constant. The values of σ_Y are taken equal to the first yield point depicted in Figure 2.

Figure 4 shows the model results and their comparison with the experimental data. The model successfully describes the work hardening behaviour at strains up to ∼0.1 at temperatures between 33 and 183 °C; above this temperature, the model shows good agreement for the entire range. At lower temperatures, the work hardening rate in the experiments decreases, whereas in the model it continues to increase. A possible explanation of this discrepancy can be that the martensite becomes saturated (from deformation twinning), and softening may occur in the β–phase, evolving to a dual phase effect. This phenomenon has not been included in the present model; a dual phase evolution can be considered in future work.

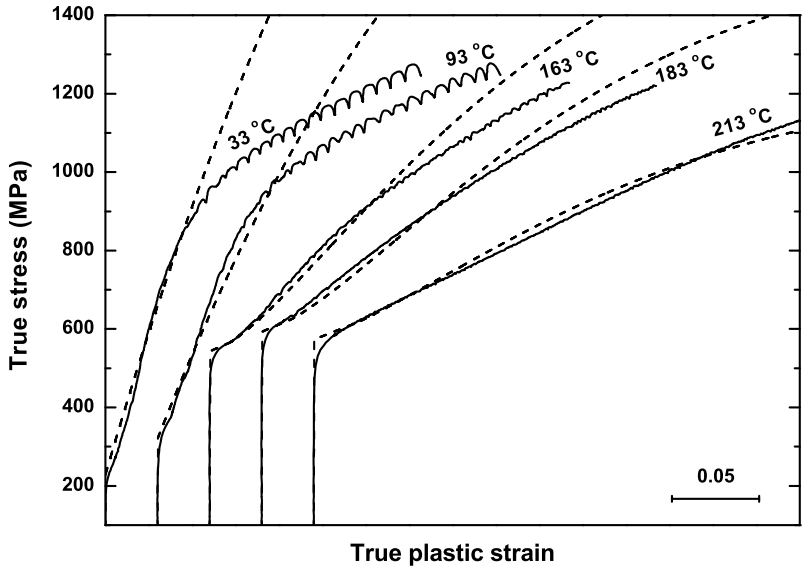

Figure 4: Comparison of the experimental stress-strain curve with the TWIN model predicted curves as function of testing temperature

6. Discussion

A combined model containing solid solution and deformation twinning effects in the martensite phase has been presented. This work extends previous theory on solid solution strengthening effects to describe diluted concentration effects. Such is achieved by modifying the analysis to describe linear dislocation–solute interactions, rather than describing volumetric solute distributions. The entropy term $T\Delta S$ (equation 4) accounts for the temperature variations in the model; this term incorporates the energy dissipation by the possible dislocation and twin configurations when they slip and grow, respectively. Previous deformation twinning description in pure materials is revisited to incorporate solid solution effects on twinning kinetics. Such is made by calibrating a constant β_1 in the energy balance for twin nucleation, and two other β_2 and β_3 in the equation for twin growth. For pure Ti β_2 and β_3 were described in terms of the crystallography of the slip and twin planes and no fitting was required [16]; β_1 was fitted as well, but its value remained constant when the model was applied to Mg and Zr. Further improvements can be made to describe such parameters more fundamentally. For instance, an additional energy term containing solute atom–dislocation

interactions (increasing stress accumulation for pile–up) in equation 8, modifying the value of γ_T^*; another energy term can be incorporated in the balance for twin growth (equation 11) to account for solute atom segregation at twin boundaries.

The model predicts a higher work hardening rate at moderate strains in the low temperature range (33–183 °C), whose discrepancy can be explained by a potential stress attenuation effect that occurs in austenite, as it is less ductile than the martensite phase. However, this interpretation has to be experimentally confirmed and modifications in the model have to be made to incorporate dual phase effects. On the other hand, the model predicts a transition from deformation twinning (in the martensite phase) to pure slip at ∼250 °C, being this temperature in good agreement with the experimental observation that SIM disappears at ∼233 °C and no hexagonal phase is left.

The combination of temperature dependent compression testing with the prediction of martensite start temperature, and the modelling of martensite deformation twinning can all be combined for alloy design. The results presented in this work demonstrate that the M_s prediction models presented by Neelakantan *et al.* [26] can be effective in conceiving new alloys wherein SIM response is tailored. This, in combination with the plasticity model presented above, may lead to design for plasticity response. Eventually, this may lead to the conception of new systems displaying optimised strength/ductility relationships. Due to the unique ability of the model to incorporate temperature effects, the work can even be applied to the design of novel hot forming processes.

7. Conclusions

1. The temperature dependence of the stress-induced martensite (SIM) effect in a near β Ti-1023 alloy in its predominant β phase state has been demonstrated.
2. The ability to form SIM decreases with increase in the deformation temperature.
3. The double yield point characteristic of the SIM effect was found to disappear after ∼233 °C, which coincides well with the predicted M_s temperature of this alloy.
4. A new thermostatistical model for multicomponent deformation twinning has been applied to Ti-1023. The martensite deformation is described well, particularly when this phase is predominant.

5. The combination of the temperature-dependent SIM formation, with the model for M_s prediction, and the deformation twinning model, can be employed to tailor the mechanical properties of near β Ti alloys.
6. High and low temperature strength/ductility optimisation in Ti alloys can be carried out with the tools presented here.
7. The deformation twinning model can be further improved to incorporate dual phase effects.

Acknowledgements This research was carried out under the research framework (Project number: MC5.05206) of the Materials Innovation Institute (www.m2i.nl) in The Netherlands. We like to express our gratitude to Mr. Javier Vara and Mr. Nacho Ruiz Oliva for the experimental support. E.I. Galindo-Nava and P.E.J. Rivera-Díaz-del-Castillo are grateful to Prof A. L. Greer for the provision of laboratory facilities. E.I. Galindo-Nava is grateful to the National Council of Science and Technology of Mexico (CONACYT) via the program "Becas para estudios de posgrado en el extranjero" and the Roberto Rocca Education Program for the provision of financial support. D. San Martin acknowledges the financial support from the Ministerio de Economia y Competitividad (Project No. MAT2010-19522).

[1] I. Polmear, Light Alloys, From Traditional Alloys to Nanocrystals, Elsevier, 2006.

[2] G. B. Olson, M. Cohen, Metallurgical Transactions A 7 (1976) 1897–1904.

[3] G. B. Olson, M. Cohen, Metallurgical Transactions A 7 (1976) 1905–1914.

[4] G. B. Olson, M. Cohen, Metallurgical Transactions A 7 (1976) 1915–1923.

[5] M. Militzer, Science 298 (2002) 975–976.

[6] T. W. Duerig, J. Albrecht, D. Richter, P. Fischer, Acta Metallurgica 30 (1982) 2161–2172.

[7] T. Grosdidier, C. Roubaud, M. . Philippe, S. Zaefferer, M. Zandona, E. Gautier, Y. Combres, Journal De Physique.IV : JP 6 (1996) C1–435–C1–444.

[8] J. D. Cotton, J. F. Bingert, P. S. Dunn, R. A. Patterson, Metallurgical and Materials Transactions A 25 (1994) 461–472.

[9] H. M. Flower, in: G. Lutjering, U. Zwicker, W. Bunk (Eds.), Deutch Gesellschaft fur Metallkunde e.v., Munich, Germany, volume 3, pp. 1651–1656.

[10] T. Grosdidier, Y. Combres, E. Gautier, M. . Philippe, Metallurgical and Materials Transactions A: Physical Metallurgy and Materials Science 31 (2000) 1095–1106.

[11] S. Ishiyama, S. Hanada, O. Izumi, ISIJ International 31 (1991) 807–813.

[12] P. Laheurte, A. Eberhardt, M. J. Philippe, Materials Science and Engineering A 396 (2005) 223–230.

[13] T. W. Duerig, G. T. Terlinde, J. C. Williams, Metallurgical Transactions A 11 (1980) 1987–1998.

[14] S. Neelakantan, D. San Martin, P. E. J. Rivera-Díaz-Del-Castillo, S. Van Der Zwaag, Materials Science and Technology 25 (2009) 1351–1358.

[15] E. Galindo-Nava, P. Rivera-Díaz-del-Castillo, Int. J. Plas. (2012. In press: 10.1016/j.ijplas.2013.02.002).

[16] E. Galindo-Nava, P. Rivera-Díaz-del-Castillo, Acta Mater. (submitted).

[17] U. Kocks, H. Mecking, Prog. Mater. Sci. 48 (2003) 171–273.

[18] E. Galindo-Nava, J. Sietsma, P. Rivera-Díaz-del-Castillo, Acta Mater. 60 (2012) 2615–2624.

[19] E. Galindo-Nava, P. Rivera-Díaz-del-Castillo, Mater. Sci. Eng. A 543 (2012) 110–116.

[20] Q. Sun, S. Song, R. Zhu, H. Gu, Journal of Materials Science 37 (2002) 2543–2547.

[21] F. Humphreys, M. Hatherly, Recrystallization and related annealing phenomena, Elsevier, 2004.

[22] R. Reed, The superalloys: Fundamentals and applications, Cambridge University Press, 2006.

[23] A. Argon, Strengthening mechanisms in crystal plasticity, Oxford University Press, 2008.

[24] K. Otsuka, X. Ren, Progress in Materials Science 50 (2005) 511–678.

[25] J. Patel, M. Cohen, Acta Metallurgica 1 (1953) 531–538.

[26] S. Neelakantan, P. E. J. Rivera-Díaz-del Castillo, S. van der Zwaag, Scripta Materialia 60 (2009) 611–614.

[27] P. Bania, in: D. Eylon, R. R. Boyer, D. A. Voss (Eds.), Beta Titanium Alloys in the 1990's, TMS Annual Meeting, Warrendale, PA, USA, volume 1, pp. 6–10.

[28] T. Zhou, M. Aindow, S. P. Alpay, M. J. Blackburn, M. H. Wu, Scripta Materialia 50 (2004) 343–348.

[29] D. Lide, CRC Handbook of Chemistry and Physics, CRC Press, 2008.

[30] E. Galindo-Nava, P. Rivera-Díaz-del-Castillo, Mater. Sci. Eng. A 558 (2012) 641.

[31] O. Le-Bacq, F. Willaime, Phys. Rev. B 59 (1999) 8508–8515.